Earth and Planetary Science Letters, 75 (1985) 297–310
Elsevier Science Publishers B.V., Amsterdam – Printed in The Netherlands

[1]

A refractory inclusion in the Kaba CV3 chondrite: some implications for the origin of spinel-rich objects in chondrites

Bruce Fegley, Jr. [1] and Jeffrey E. Post [2,*]

[1] *Department of Earth, Atmospheric and Planetary Sciences and Ceramics Processing Research Laboratory, Massachusetts Institute of Technology, Cambridge, MA 02139 (U.S.A.)*
[2] *Department of Geological Sciences, Harvard University, 24 Oxford Street, Cambridge, MA 02138 (U.S.A.)*

Received March 13, 1985; revised version accepted July 13, 1985

The first detailed petrographic and mineralogical study of a Ca, Al-rich inclusion (CAI) from the Kaba CV3 chondrite is reported. This "fine-grained" CAI contains abundant small, rounded, rimmed, spinel-rich objects which have important features in common with the spinel-rich objects in other carbonaceous and ordinary chondrites. These nodules are interpreted as fractionated distillation residues of primitive dust. However, the available data do not unambiguously rule out a condensation origin for at least some of these objects. Finally, the preservation of distinct diopside-hedenbergite rims on the spinel-rich bodies and the small grain size of many minerals in the CAI matrix material both suggest that the CAI accreted cool and had a relatively cool thermal history in the Kaba parent body.

1. Introduction

The Kaba CV3 chondrite fell near the village of Kaba, Hungary, on the evening of April 15, 1857 [1]. It was described by Török (1858), who noted the occurrence of "white spots" 10–15 mm long on the stone's surface [1]. These "spots" (which are illustrated in the figures accompanying Török's paper) were later studied by Sztrokay et al. [2, and references therein] who reported that they contained Mg-Al spinel and enstatite. This was the first report of spinel in meteorites. We believe that Török's observations in 1858, more than a century before the modern descriptions of Ca, Al-rich inclusions (CAI's) in the Allende, Lancé, and Vigarano CV3 chondrites [3–5], may be the first report of CAI's in meteorites.

However, no further studies of CAI's in Kaba have appeared since Sztrokay's petrographic study. The only relevant work of which we are aware is an estimate of CAI modal abundances in Kaba [6] and a compilation of some CAI bulk compositions [7]. The difficulty of obtaining samples of Kaba (the main mass of which is in a church college in Debreczen, Hungary) is undoubtedly at least partially responsible for the lack of studies of CAI's in this meteorite. Fortunately, while studying CV3 meteorite matrix, J.A. Peck observed a relatively large "fine-grained" CAI in a Kaba polished section in J.A. Wood's collection. We have been able to study this CAI and in this paper we present the results of our work, which is the first detailed mineralogical study of a CAI in Kaba.

2. Observational methods

The polished section containing the spinel-rich CAI was studied by scanning electron microscopy (SEM) and by electron probe microanalysis (EPMA). Mineral analyses were performed at the Department of Geological Sciences, Harvard University, using an automated Cameca MBX EPMA operated at 15 kV and approximately 15 nA, with on-line Bence-Albee data reduction. Natural and synthetic minerals were used as standards. Vanadium analyses were empirically corrected for the Ti(K/β) interference as described by Kornacki and Wood [8]. Back-scattered electron imaging (BSE) and energy dispersive spectroscopy (EDS) were used concurrently to select and identify mineral grains for analysis. The inclusion was pho-

* Present address: Department of Mineral Sciences, NHB 119, Smithsonian Institution, Washington, DC 20560, U.S.A.

0012-821X/85/$03.30

tographed in reflected light and studied in detail by secondary electron imaging on an AMR Model 1000 SEM.

3. Petrographic description

The entire CAI is approximately 3.6 × 4.7 mm and is irregularly shaped. Some small sections are separate from the main body of the inclusion but may be connected to it in the third dimension. Completely mantling the outside of the entire inclusion is a clastic rim sequence like those described by MacPherson and Grossman [9] surrounding "fluffy" Type A inclusions in Allende. The rim consists of at least two different layers; a fine-grained inner layer surrounded by a coarse-grained layer. The Kaba CAI appears similar to TS12F5, which is an Allende CAI intermediate between "fluffy" Type A's and "fine-grained" CAI's [9]. Fig. 1 is a BSE mosaic of the Kaba CAI and Fegley et al. [10] show a reflected light photomicrograph.

Fig. 1 shows that the CAI is composed of several constituents which are mineralogically and texturally distinct from each other. They are heterogeneously distributed in the inclusion, and have different shapes, sizes, and chemical compositions. Spinel-rich objects occur singly or in groups (Fig. 1). They are Al-rich, with prominent core-and-rim structures (Fig. 2A), and may be rounded, elongated along one axis (football or egg-shaped), or irregularly shaped ("wormy") (Fig. 2B). A few have large cracks (0.5–1.0 × the object's apparent diameter) running through them (Fig. 2C), and others have sections (≈ 1/3 × the total circumference) of their rim removed (Fig. 2D). Their apparent diameters are in the range 50–200 μm, and the apparent sizes (longest dimension) of the "wormy" objects are similar.

Typically these objects have $MgAl_2O_4$-spinel

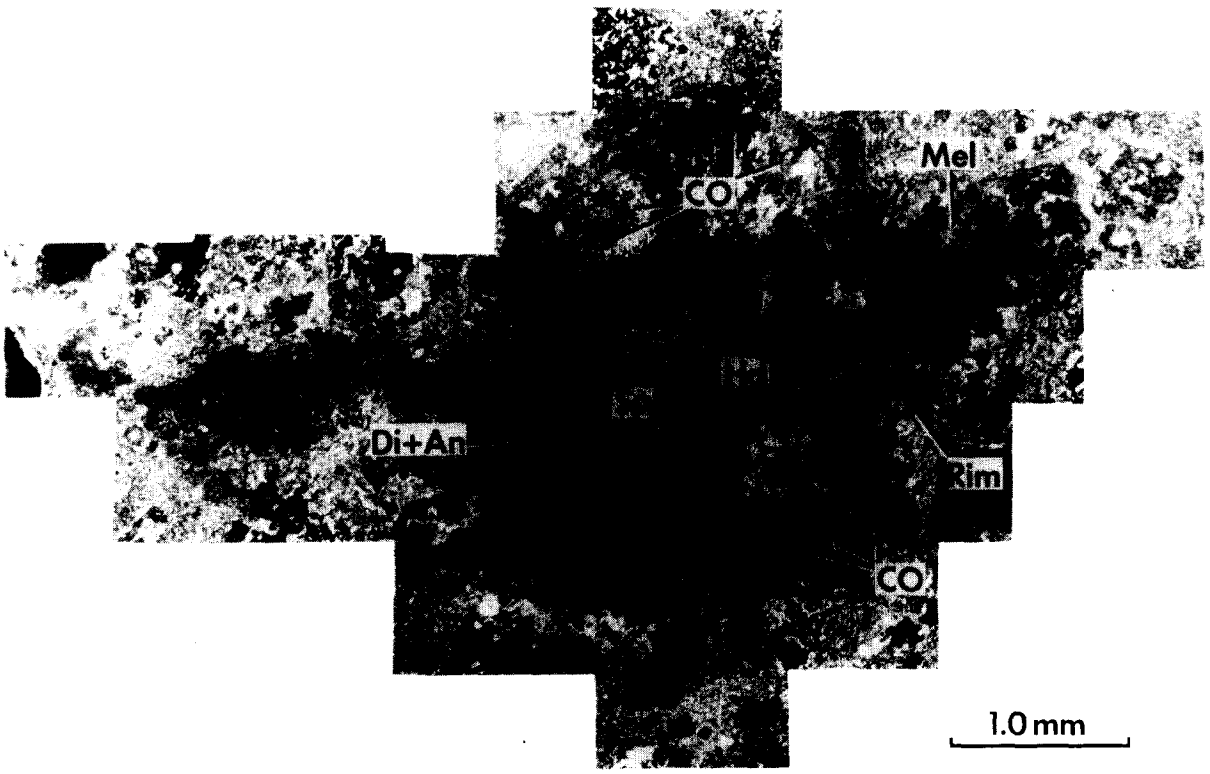

Fig. 1. Back-scattered electron mosaic of the Kaba CAI. Spinel-rich concentric objects (*CO*), hedenbergite (*Hd*), diopside (*Dp*), anorthite (*An*), melilite (*Mel*), and "wormy" spinels (*Sp*) are heterogeneously distributed throughout the CAI. A section of the clastic rim is also labelled.

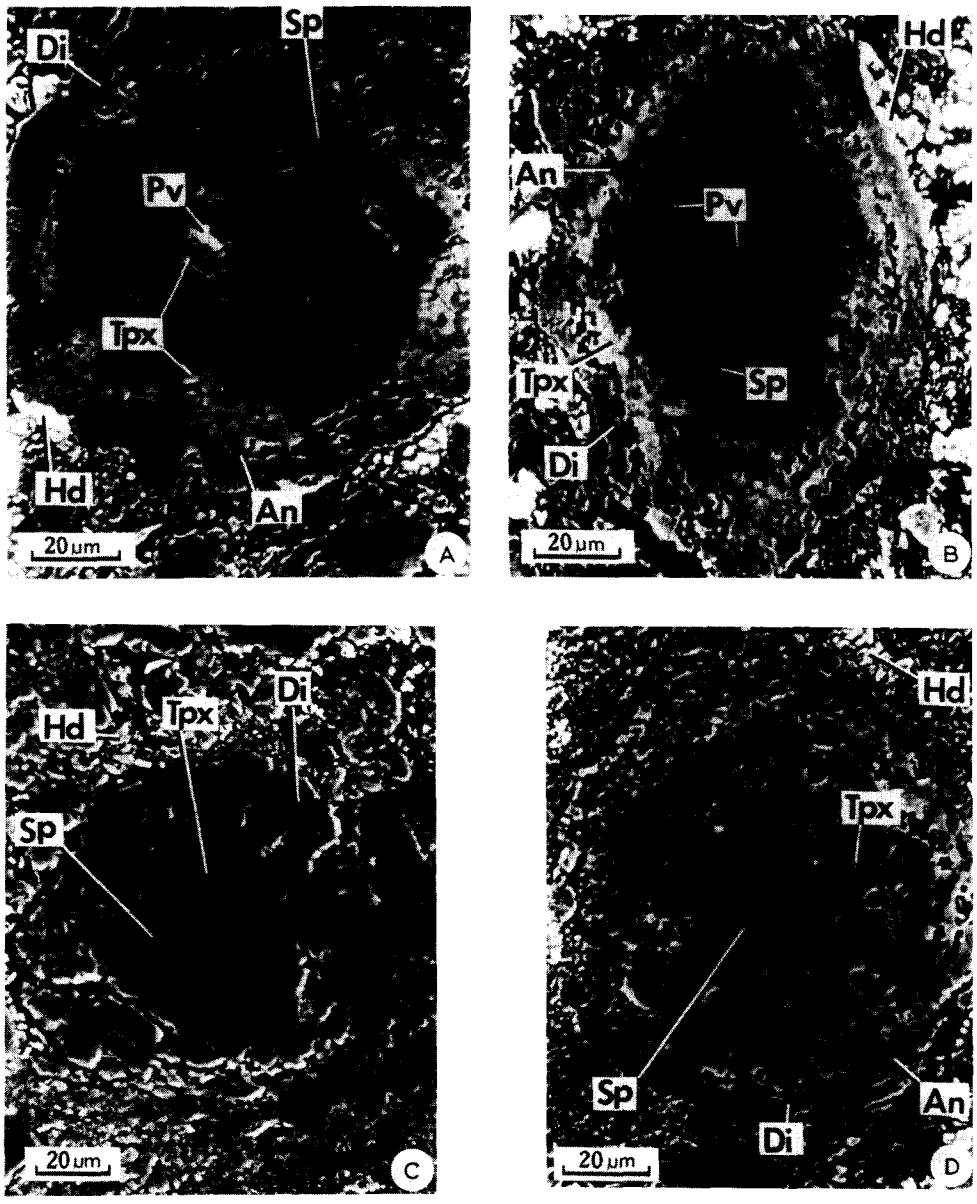

Fig. 2. SEM micrographs of individual spinel-rich concentric objects. A, B, and D are back-scattered electron images; C is a secondary electron image. A. CO1 contains spinel (*Sp*), Ti-Al pyroxene (*Tpx*), and perovskite (*Pv*) in its core. Porosity is ≈ 6% of core volume. A complex Ti-Al pyroxene, anorthite, diopside, hedenbergite rim surrounds the core. B. CO12 has a core with minor perovskite and ≈ 7% porosity. C. CO3 is fractured and has part of its rim missing. D. CO13 has spinel, Ti-Al pyroxene, minor perovskite and ≈ 6% porosity in its core. Part of the rim is also missing.

cores with variable amounts of Ti-Al-pyroxene, trace perovskite or ilmenite (grain size $\leqslant 8$ μm), and porosity (pore size ≈ 1–20 μm). However, one has a Ca, Si-rich core with a spinel rim and another has a spinel core apparently inside a hollow shell (Fig. 3A, B). The "grain" size and texture of the spinel and Ti-Al-pyroxene intergrowth varies from object to object. In some, the two minerals are intergrown on a scale of a few microns; in others the minerals are segregated on a scale of tens of microns. Ilmenite apparently occurs preferentially in the Ti-Al-pyroxenes; both perovskite

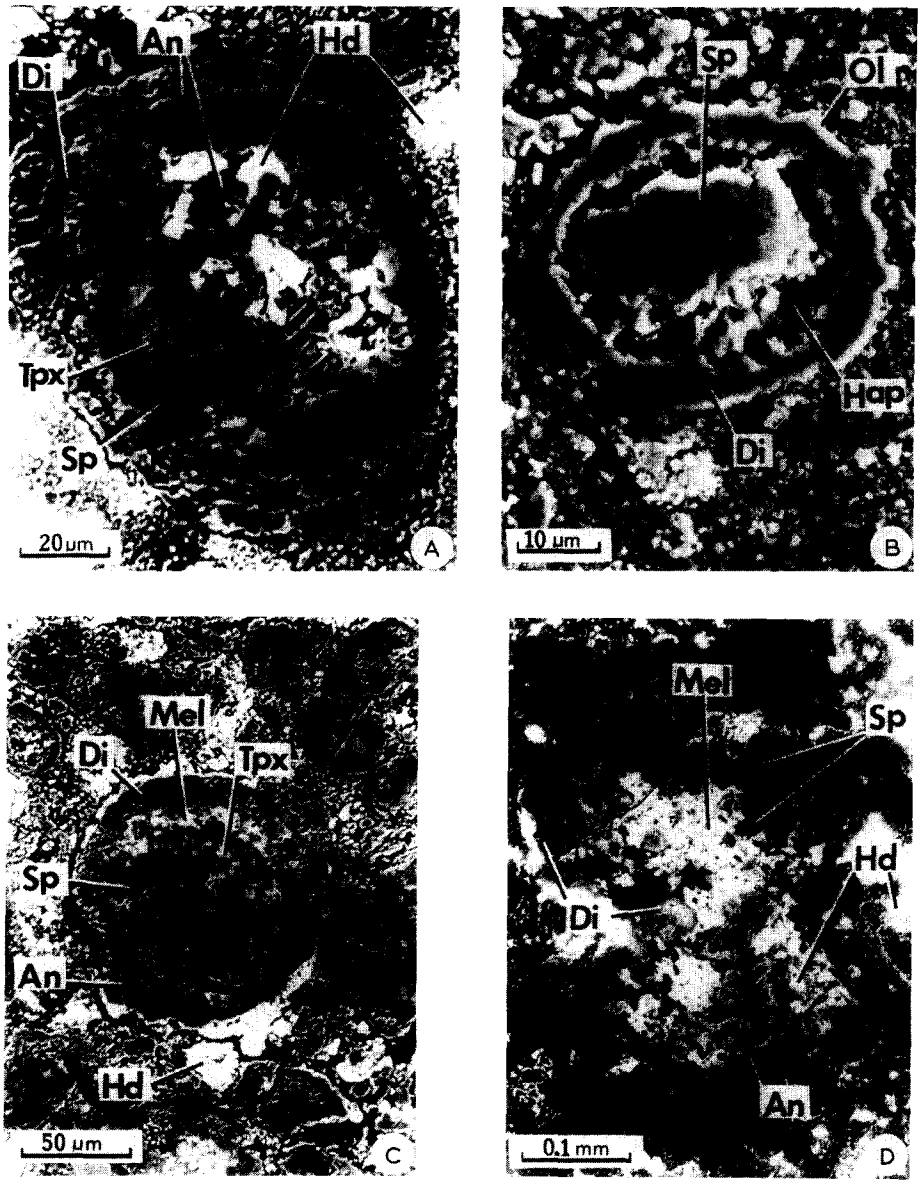

Fig. 3. A–C are SEM micrographs of individual spinel-rich concentric objects. B is a secondary electron image, A, C, D are back-scattered electron images. Abbreviations as in Figs. 1 and 2. A. CO14 has a Ca, Si-rich core rimmed by spinel. B. CO10 contains spinel rimmed by a HAP-type phase, diopside and olivine (*Ol*). (C) CO2 showing the surrounding matrix material. Melilite occurs along one section of the rim. D. Melilite grain MEL1 displays a complex structure with extensive alteration to diopside, anorthite, and hedenbergite.

and ilmenite are present in amounts $< 1\%$ by volume. Point counting and the line intercept method [11] indicate that the porosity also occurs preferentially in the Ti-Al-pyroxenes. This porosity may have several different origins. Pores that are associated with cracks or that truncate crystals in an irregular fashion may be polishing artifacts (e.g., see MacPherson et al. [12]). However, many pores do not have these characteristics, are rounded, and are considered to be primary. Unidentified Na, K, Cl, S-rich phase(s) were found in some pores by EDS and are probably alteration

TABLE 1

Rimmed, spinel-rich objects: petrography and chemistry

	CO1	CO2	CO3	CO8	CO10	CO11	CO12	CO13	CO14
Apparent diameter (μm)	117	125	100	125	40×45	70	138×94	106	100×125
Apparent core diameter (μm)	83	88	88	100	13×23	53	100×62	80	81×88
Rim thickness (μm)	17	13–18	6	13	13×15	9	13×19	13	11
Core [a] mineralogy	82% sp 18% pyx (18-μm pv grain)	66% sp 34% pyx	70% sp 30% pyx	51% sp 49% pyx	sp, minor Ti-pex, surrounded by HAP	94% sp 6% pyx	100% sp (3 tiny pv grains)	78% sp 22% pyx	an, hd, sp, Ti-pyx
Core [b] CaO/Al_2O_3 (wt.%)	0.08	0.16	–	0.24	–	0.03	0.01	0.10	–

[a] Determined using rastered beam EPMA, assuming only spinel (sp) and Ti-pyroxene (pyx) to be present in the core. Independently estimates of the spinel and pyroxene modal abundances made by point counting agree within 10% in the worst cases (CO1 and CO11) and within 2% in the best cases (CO8 and CO9). pv = perovskite.

[b] The solar CaO/Al_2O_3 ratio is 0.79.

products. Secondary electron imaging shows material inside some pores, but the crystalline forms cannot be identified. Pt-metal nuggets were only rarely observed; trace sulfides (possibly including MoS_2) were also seen in one concentric object. Neither hibonite nor $CaAl_4O_7$ were observed; however, hibonite was observed in another Kaba sample (G.J. MacPherson, personal communication).

The complex rim sequence (thickness 10–20 μm) surrounding the cores of the spinel-rich objects is similar to the Wark-Lovering rims on Allende CAI's [13]. Several "bands", each only a few microns thick, make up the rim sequence. From inside to outside the rim sequence consists of Ti-Al-pyroxene, anorthite, diopside, and hedenbergite. The composition of the diopside layer (which is typically the thickest rim) grades from more aluminous to less aluminous progressing outward. Both the anorthite and hedenbergite rims may be discontinuous; one or both are absent from the rim sequences on some spinel-rich bodies. Magnetite and fayalitic olivine were rarely observed adhering to the outside of the rim layers; however, these may be bits of inclusion matrix [8] and not true rim layers. It is an oversimplification to describe the rim layers as monomineralic. There is often mixing between the anorthite and diopside layers, especially in bulges on some spinel-rich objects, (e.g. Fig. 2A). Finally, unidentified Mg-Al-Si-rich phases with 1–3 wt.% Na_2O and 0.2–0.7 wt.% K_2O are also present in dark areas (in BSE imaging) and pores near the inner edges of some rim sequences. These phases possibly are analogous to the high-aluminum and low-aluminum phyllosilicates (HAP and LAP) reported by Cohen et al. [14] to occur in cracks and pores of rims and inclusion matrix in Mokoia. Table 1 summarizes some of the major features of spinel-rich objects and also helps to give some indication of the observed variability of their mineralogical and morphological features.

Melilite grains occur in different areas of the CAI; there is no apparent relationship between the grains and surrounding matrix. The melilite grains are apparently extensively altered to anorthite, diopside, and hedenbergite (Fig. 3D). Spinel, which is more FeO-rich than in the cores of the spinel-rich objects, is also present in one large melilite grain (MEL1). This grain is rimmed by an irregular and discontinuous rim of spinel (20–40 μm thick), a continuous rim of diopside ($\approx$ 5 μm thick), and an outer discontinuous layer of hedenbergite. Cavities in the grain are also rimmed by hedenbergite, diopside and anorthite; some cavities are filled with hedenbergite but there is no spinel around

cavities. The interior of the grain is a mixture of anorthite and melilite. EPMA profiles show some variations in melilite composition, but the (possibly) polycrystalline grain shows no systematic zoning.

The spinel-rich objects and melilite grains are set in a porous matrix of fragments ranging in size from < 1 to 100 μm. The predominant mineral phases comprising the matrix are anorthite, diopside, hedenbergite, Fe-Ni sulfides and olivine, and they are heterogeneously distributed in the CAI. Hedenbergite veins and patches are prominent, anorthite-diopside assemblages are also commonly observed. Some matrix fragments are attached to chemically similar rims on the spinel-rich objects (Fig. 3C).

4. Mineral chemistry

The mineral compositions were generally constant within small ranges and representative analyses are listed in Table 2. Defocused beam microprobe analyses were also made on the cores of several spinel-rich objects and on matrix material. These analyses reflect the well defined segregation of refractory elements into Al-rich and Ca, Si-rich areas, i.e., into spinel-rich objects and matrix material. The defocused beam CaO/Al_2O_3 ratios for the cores of the spinel-rich nodules are listed in Table 1. More extensive discussions of mineral chemistry are given below.

4.1. Spinels

Spinel occurs in the cores of rounded, rimmed bodies and in one melilite grain (MEL1). FeO in spinel ranges from < 0.04 to 0.93 wt.% with a mean value of 0.26 wt.%. There are subtle but possibly significant differences in the FeO contents of spinels in the spinel-rich objects and in the melilite grain (MEL1). The latter spinels contain ≈ 0.9 wt.% FeO while the former contain less than ≈ 0.6 wt.% FeO.

Small amounts of V_2O_3, Cr_2O_3, CaO, TiO_2, and SiO_2 were found in all spinels. The mean contents (and observed ranges) are V_2O_3, 0.36 wt.% (0.23–0.54 wt.%); Cr_2O_3, 0.17 wt.% (0.09–0.25 wt.%); CaO, 0.11 wt.% (0.02–0.32 wt.%); TiO_2, 0.28 wt.% (0.05–0.45 wt.%); and SiO_2, 0.09 wt.% (0–0.24 wt.%). There is very little variability in the V_2O_3 and Cr_2O_3 contents of spinels within a single spinel body or between different spinel objects (typically < 0.05 wt.%). However, there is slightly more variability (≈ 0.08 wt.%) in the FeO contents. There is no correlation between FeO and V_2O_3 in the spinels but there is a weak positive correlation (correlation coefficient > 0.93) between FeO and Cr_2O_3 for FeO concentrations $> 0.2\%$. The most significant features of the spinel analyses are their low FeO contents, small variability in FeO and minor elements, and very similar minor element concentrations.

4.2. Melilite

Melilite occurs as separate grains and on one side of the core of one spinel-rich object (Fig. 3C). The grains are often found in association with anorthite, diopside, and hedenbergite. The melilites are relatively gehlenitic (Åk $\approx$ 10–30) and have a mean composition of $Åk_{18}$. This composition is at the low-Åk end of the range of compositions in Type A inclusions and is similar to the compositions found in "fluffy" Type A CAI's [9]. Some melilites contain 0.1–0.3 wt.% FeO and trace amounts of Na_2O. They also typically contain < 0.05 wt.% each V_2O_3, Nb_2O_5 and Y_2O_3, < 0.08 wt.% ZrO_2, and < 0.12 wt.% each Ce_2O_3, BaO, and SrO. However one grain contains 0.15 wt.% Ce_2O_3.

4.3. Mg-rich clinopyroxenes

Mg-rich clinopyroxenes are abundant in this inclusion and occur in several different mineral associations. They occur intergrown with spinel in the cores of spinel-bearing objects, in the Wark-Lovering type rims around these bodies and in the porous matrix material. Following the classification used by Kornacki and Wood [8] we refer to Al-bearing clinopyroxenes which contain < 1 wt.% TiO_2 as Al-diopside and Al-bearing clinopyroxenes which contain ≥ 1 wt.% TiO_2 as Ti-Al pyroxene. The mineral sequence (interior to exterior) in the Wark-Lovering type rims around the spinel-rich bodies is typically Ti-Al pyroxene, anorthite, Al-diopside, and hedenbergite. The Al-diopsides analyzed have Al_2O_3 contents ranging from ≈ 0.6 to 11.2 wt.%, and TiO_2 contents ranging from 0 to ≈ 0.6 wt.%. (All Ti in all pyroxene

TABLE 2

Representative analyses of selected minerals

Mineral	pv	sp	mel	tpx(R)	tpx(C)	dp	hed	an	ol	wo	andr
SiO_2	0.76	0.11	25.70	32.39	35.44	53.89	49.13	43.19	41.85	50.19	37.25
TiO_2	55.78	0.13	0.00	12.69	10.59	0.52	0.00	0.15	0.00	0.03	0.07
Al_2O_3	2.18	69.84	30.84	24.28	22.43	2.61	0.60	34.73	0.00	0.86	1.55
V_2O_3	< 0.07	0.40	0.00	0.27	0.16	0.07	< 0.06	< 0.06	0.00	< 0.07	< 0.07
Cr_2O_3	n.a.	0.18	0.00	< 0.06	< 0.05	< 0.05	< 0.05	0.00	0.23	0.00	< 0.06
FeO	0.07	0.59	0.00	< 0.04	< 0.04	0.23	25.36	0.14	1.66	5.98	27.71 [b]
MgO	0.84	28.48	2.41	6.75	7.92	19.06	2.18	1.47	55.36	5.23	1.02
CaO	38.89	0.10	40.89	24.60	23.94	23.38	21.98	19.48	0.05	36.09	31.55
Na_2O	n.a.	n.a.	0.00	0.02	0.03	0.07	0.03	0.08	0.02	0.03	0.05
MnO	n.a.	0.00	n.a.	< 0.03	0.00	0.00	0.51	< 0.03	n.a.	0.27	0.25
Total	99.36 [a]	99.83	99.84	101.00	100.51	99.83	99.79	99.24	99.17	98.68	99.45
Oxygens	*3*	*4*	*7*	*6*	*6*	*6*	*6*	*8*	*4*	*3*	*12*
Si	0.017	0.002	1.173	1.187	1.294	1.936	1.993	2.016	0.996	0.980	3.099
Ti	0.943	0.002	0.000	0.350	0.291	0.014	0.000	0.005	0.000	0.000	0.004
Al	0.058	1.964	1.659	1.049	0.966	0.111	0.029	1.911	0.000	0.020	0.152
V	–	0.008	0.000	0.010	0.006	0.002	–	–	0.000	–	–
Cr	–	0.003	0.000	–	–	–	–	0.000	0.004	0.000	–
Fe	0.001	0.012	0.000	–	–	0.007	0.861	0.005	0.033	0.098	1.735
Mg	0.028	1.013	0.164	0.369	0.431	1.020	0.132	0.102	1.965	0.152	0.126
Ca	0.936	0.002	2.000	0.966	0.937	0.900	0.956	0.975	0.001	0.755	2.813
Na	–	–	0.000	0.002	0.002	0.005	0.003	0.007	0.001	0.001	0.008
Mn	–	0.000	–	–	0.000	0.000	0.018	–	–	0.004	0.018
Total	1.990 [a]	3.006	4.996	3.933	3.927	3.995	3.992	5.021	3.000	2.010	7.955

Key: an = anorthite, andr = andradite, dp = diopside, hed = hedenbergite, mel = melilite, ol = olivine, pv = perovskite, sp = spinel, tpx = Ti-Al pyroxene, wo = wollastonite; R, C = rim, core of a concentric object

[a] Sums include < 0.05% HfO_2, Y_2O_3; < 0.10% BaO, SrO; 0.00% ZrO_2; 0.31% Nb_2O_5, and 0.53% Ca_2O_3 (0.003 atom units Nb and 0.004 atom units Ce).

[b] All Fe as Fe_2O_3

n.a. = not analyzed.

analyses is assumed to be TiO_2; however the generally low cation sums of 3.93–3.96, particularly for Ti-rich Ti-Al pyroxenes suggest that some Ti is present as Ti^{3+}.) Two analyses around the circumference of the Al-diopside rim on one spinel-rich object show different TiO_2 contents (0, 0.52 wt.%), Al_2O_3 contents (0.66, 2.61 wt.%), V_2O_3 contents (0, 0.07 wt.%), and FeO contents (1.13, 0.23 wt.%). The observed variations may be due to extremely fine intergrowths of the Al-diopside with another mineral or minerals. Indeed, the BSE imaging does show some intermixing of the anorthite and diopside layers (Fig. 2A). However, every effort was made to avoid analyzing obviously heterogeneous pieces of the rim, and BSE imaging was consistently used during analyses.

Ti-Al pyroxenes in the cores and rims of the spinel nodules were analyzed for possible compositional trends which may be diagnostic of the modes of origin of the pyroxenes. One observation is that the rims around the "wormy" spinel-rich bodies are mainly Al-poor diopside with very little Ti-Al pyroxene. Another observation is that the mean Al_2O_3 and TiO_2 concentrations (and observed ranges) for 32 analyses of the more rounded spinel-rich objects are Al_2O_3 22.2 wt.% (9.1–30.3 wt.%) and TiO_2 9.8 wt.% (2.2–14.4 wt.%). There are no statistically significant differences in the concentrations of Al_2O_3 and TiO_2 between the Ti-Al pyroxenes in the cores and rims of the spinel bodies. Mean concentrations from 22 analyses of pyroxenes in 4 cores are 22.6 ± 2.0 wt.% and 10.6 ± 2.2 wt.%, respectively (uncertainties are $\pm 1\sigma$), those from 10 analyses in 5 rims are 20.9 ± 7.4 wt.% and 7.2 ± 3.2 wt.%, respectively. The mean Al_2O_3 and TiO_2 concentrations for the Kaba Ti-Al

pyroxenes fall within the upper range observed in Allende Type B1 pyroxenes by Wark and Lovering [15], and are higher than observed in Allende spinel-rich CAI's by Kornacki and Wood [8]. A separate but related question is whether the Ti-Al pyroxenes in the core and rim of a single spinel body have similar or different compositions. This is difficult to answer unambiguously because the intimate intergrowth of spinels and pyroxenes (with pyroxenes having sizes $\leqslant 5$ μm) in the cores of these objects, the small thicknesses of pyroxene rims (≈ 1–5 μm), and the differential polishing of spinels and pyroxenes make it difficult to obtain good analyses on any one object. The data for two different spinel bodies show similar Al_2O_3 and TiO_2 concentration ranges in the core and rim of the first one and lower ranges in the rim than in the core of the second one. Finally, we searched for possible compositional variations among pyroxenes in the core of a single spinel body and among pyroxenes in the cores of different spinel-rich objects. Variations of ≈ 8 wt.% TiO_2 and ≈ 5 wt.% Al_2O_3 occur within the core of a single spinel-rich body. These are not related to the location of the pyroxene inside the core. Compositional variations of similar magnitude occur among pyroxenes in the cores of different spinel-rich objects.

4.4 Other minerals

Other minerals studied by EPMA include hedenbergite, anorthite, olivine, wollastonite, and andradite. Hedenbergite is inhomogeneously distributed throughout the inclusion in veins and patches, occurs as the outer layer in the Wark-Lovering type rims on spinel-rich objects, and around pores in the large melilite grain (MEL1). One object studied has hedenbergite, anorthite, and Ti-Al pyroxene in the core (Fig. 3A). Seventeen analyses of hedenbergite in these various assemblages showed no systematic compositional variations; the observed ranges of composition were $\approx Dp_{60}Hd_{40}$ to Hd_{100}. The hedenbergite is heterogeneous at about the 5 μm scale with the compositions scattering within the above limits. Anorthite occurs in the rim sequence on spinel-rich bodies, in the porous matrix material, in the core of one spinel body (Fig. 3A), and in the few melilite grains in the inclusion. It is usually $An_{>99}$

TABLE 3

Analyses of Mg-Al-Si-rich phases in Kaba and Mokoia

	High-aluminous phase (HAP) [cations/14(O)]		Low-aluminous phase (LAP) [cations/22(O)]	
	Kaba [a]	Mokoia [b]	Kaba [c]	Mokoia [d]
Al	1.01 (0.28)	0.79 (0.21)	1.66 (0.00)	1.10 (0.12)
Si	2.99 (0.28)	3.21 (0.21)	6.34 (0.00)	6.90 (0.12)
Tetrahedral	4.00	4.00	8.00	8.00
Al	2.08 (0.22)	1.77 (0.18)	0.60 (0.08)	0.24 (0.08)
Ti	0.02 (0.02)	0.03 (0.03)	–	0.02 (0.01)
Fe	2.52 (0.29)	2.83 (0.20)	0.89 (0.30)	0.32 (0.02)
Mg	0.39 (0.16)	0.28 (0.06)	4.44 (0.40)	5.42 (0.05)
Octahedral	5.01	4.91	5.93	6.00
Ca	0.21 (0.09)	0.19 (0.05)	0.12 (0.02)	0.10 (0.05)
Na	0.42 (0.14)	0.68 (0.14)	0.52 (0.27)	0.28 (0.06)
K	0.05 (0.02)	0.10 (0.03)	0.24 (0.03)	0.31 (0.02)
Interlayer	0.68	0.97	0.88	0.69
Total	9.69	9.88	14.75	14.69

[a] Average of 7 analyses; standard deviations in parentheses.
[b] Cohen et al. [14] average of 4 analyses.
[c] Average of 2 analyses.
[d] Cohen et al. [14] average of 5 analyses.

but one has the composition $An_{75}Ab_{25}$ (Fig. 3A). Olivine in the porous matrix material ranges from Fa_5 to Fa_{90} with a tendency to be forsteritic, but not enough data were taken to determine a significant mean composition. Wollastonite and andradite, which are apparently trace phase, were also identified in the outer edge of the rim and in the core, respectively, of one spinel body. Finally, perovskite is a rare mineral found as tiny grains (typically < 5 μm) enclosed in spinel in the cores of the spinel-rich objects. Only one grain was large enough (≈ 8 μm) to analyze; the analysis is given in Table 2. The high Al_2O_3 concentration of 2.18 wt.% and the Al/Mg cation ratio of 2.1 suggest the possibility of some contamination by surrounding spinel; however, the cation sum of 1.990 indicates good stoichiometry. Variable Ce concentrations ranging from < 0.12 wt.% to 0.64 wt.% Ce_2O_3 were also observed in this perovskite grain.

We found Mg, Al silicates in cracks and pores near the inner edges of Wark-Lovering type rim sequences and in pores in the inclusion matrix that typically yielded low EPMA summations (75–85%). The low summations might result from high sample porosity and the fact that the phases occur in cracks or from the presence of water in the compounds. Analyses indicate that there are at least two different phases, one having a higher Al content than the other, which appear to be analogous to the high- and low-aluminous phases described by Cohen et al. [14] in Mokoia, which also yielded EPMA summations near 80%. Table 3 shows that the average compositions of the Mg-Si-Al-rich phases in Kaba are very similar to that of the high- and low-aluminous phases from Mokoia, the major differences being fewer interlayer cations and more Al in the high-aluminous phase, and more Al and Mg in the low-aluminous phase from Kaba. Unambiguous identification of the phases was not possible because the grains are too small (< 10 μm) to be removed for X-ray diffraction. Cohen et al. [14], however, concluded on the basis of crystal chemistry and X-ray diffraction studies of a single grain that the high-aluminous phase might be an Al-serpentine or very fine-grained mixture of minerals, and that the structural formula of the low-aluminous phase is almost identical to the idealized formula of trioctahedral montmorillonite.

5. Discussion

5.1. Comparisons to Allende and Mokoia

Several important features are common to rimmed, spinel-rich objects in Kaba, Allende, and Mokoia. Spinel-rich bodies in the Kaba CAI have a variety of shapes but are commonly rounded. Allende [8,13,14,16–18] and Mokoia [14] spinel-bearing objects also have various shapes but many are rounded. "Wormy" spinel-rich objects occur in all three meteorites. Spinel-rich objects in all three meteorites also fall into the same (broad) size range ≈ 10–500 μm (e.g., refer to figures in [8,9,13,14,16–18]. The prominent core and rim structure with spinel-rich cores and Ca, Si-rich rims is another common feature [8,13,14,17,18] but some spinel-rich nodules in Allende "fluffy" Type A inclusions contain melilite in their cores [9]. However, others such as the spinel-rich nodules found in the core of the Allende "fluffy" Type A inclusion TS12F5 [9] consist of spinel cores rimmed by diopside and contain no melilite. The rim thicknesses ($\leqslant 20$ μm) and the presence of several different mineralogical bands within the rim are other important similarities. To be sure, two objects which are exceptions to the above (Fig. 3A, B) were observed. However, our basic conclusion is that important morphological similarities are common to the spinel-rich objects in this Kaba CAI and those in Allende [8,13,14,16–18] and Mokoia [14]. The matrix material in this CAI and in the Allende and Mokoia CAI's also have common features [8,14,16]. They are Ca, Si-rich, contain the same minerals (diopside, melilite, hedenbergite, sulfides), and have similar morphologies and range of grain sizes.

Mineralogical similarities also exist between the spinel-rich objects in the three meteorites. Pt-metal nuggets are rarely observed in these bodies in spinel-rich CAI's in Kaba, Allende [8], and Mokoia [14]. Ti-Al pyroxene, diopside, anorthite, and hedenbergite may occur in the rims on the spinel bodies in all three meteorites. Also the clinopyroxenes in the rims of the spinel bodies in all three meteorites grade from Ti-Al pyroxenes to Al-diopsides from interior to exterior. The minor element chemistry of spinels in Kaba and Allende spinel-rich CAI's [8] are also similar in some respects; both have similar V_2O_3 and Cr_2O_3 mean

concentrations although Allende spinels contain more ZnO. Melilite is rarely observed in the spinel-rich objects in Kaba and Mokoia but it is more common in the spinel-rich nodules of some Allende "fluffy" Type A CAI's [9]. However, Kornacki and Wood [16] classify "fluffy" Type A CAI's differently than the spinel-rich CAI's where melilite is much less abundant.

At the same time, subtle but possibly significant compositional differences tend to distinguish between the spinel-rich objects in the three meteorites. Those in Kaba and Mokoia [14] contain FeO-poor spinel; those in Allende contain pleonaste spinel [8]. A feldspathoid rim occurs on objects in Allende; no such rim was observed on spinel-rich nodules in Mokoia [14] and Kaba. Instead a Mg-Al silicate rim is present on spinel-rich objects in these two meteorites. The Ti-Al pyroxenes in Allende spinel-rich inclusions generally contain < 3 wt.% TiO_2 and < 12 wt.% Al_2O_3 [8], while those in the Kaba CAI have mean concentrations of 9.8 wt.% TiO_2 and 22.2 wt.% Al_2O_3. (Only one Ti-Al pyroxene analysis was reported for fine-grained CAI's in Mokoia [14]; it is closer to the mean compositions seen in Kaba.)

5.2. *Occurrence of spinel-rich objects in other chondrites*

We conclude that the rimmed, spinel-rich objects in Kaba, Allende, and Mokoia share important common features. This similarity also extends to rimmed, spinel-cored objects in other chondrites. Cohen [19] found rimmed, spinel-cored objects in all twelve C2 and C3 chondrites studied by SEM and EPMA (Mighei, Murchison, Murray, Nagoya, Pollen, Ornans, ALHA 77306, Isna, Grosnaja, Kaba, Mokoia, and Vigarano). Spinel-bearing, concentrically rimmed objects were reported in "fine-grained" CAI's in Efremovka by Ulyanov [20]. Finally, Frost and Symes [5] described a rounded, spinel-perovskite-bearing "chondrule", which we interpret as a rimmed, spinel-rich object similar to those in Kaba, from Lancé.

Our brief review of these various rimmed, rounded, spinel-cored objects indicated that major morphological similarities (e.g., shape, size, core and rim structure, spinel cores, Ca, Si-rich rims, rim thicknesses) exist and suggests that the spinel-rich objects in CAI's in many carbonaceous and ordinary chondrites are similar to each other and to spinel-rich chondrules. Furthermore, there is an apparent continuum of rimmed, spinel-bearing objects ranging from those with only spinel in the cores (e.g., Fig. 2B) to those with mixtures of spinel and pyroxene (Fig. 2A, C, D) to those with Ca, Si-rich cores, spinel rims, and Wark-Lovering type rims (Fig. 3A). What do these observations imply for the origin of these objects?

5.3. *Origin of spinel-bearing objects*

Cohen [21] first suggested that rimmed, rounded spinel-rich objects could form during the distillation of primitive dust aggregates by partial melting and physical fractionation of Ca, Si-rich partial melts from residual spinel grains [22]. Cohen et al. [14], MacPherson et al. [12], and Kornacki and Wood [8] applied this model to the origin of spinel-rich inclusions in Mokoia, blue spinel-hibonite spherules in Murchison, and spinel-rich CAI's in Allende, respectively. We propose that this model (which is described in detail elsewhere [14,17]) is also applicable to the spinel-rich objects in Kaba.

The range of properties observed in the rimmed, rounded, spinel-cored objects in Kaba are consistent with Cohen's model. More irregularly shaped objects have $\approx 100\%$ spinel cores with almost no Ti-Al pyroxenes (Fig. 2B). More rounded and circular objects contain differing proportions of spinel and Ti-Al pyroxene, but are always spinel-rich (Fig. 2A, C, 3A, C, D). They also contain ≈ 5–10% porosity in their cores (mainly in the Ti-Al pyroxenes). This amount of porosity may be consistent with the amount produced by shrinkage due to the crystallization of a Ca, Si-bearing melt. No ΔV data have been determined for fassaitic pyroxenes, however; the ΔV for crystallization of several Ca, Si-rich minerals is of the same order of magnitude: 9% for $CaSiO_3$, 8% for $Ca_2MgSi_2O_7$, 20% for $CaMgSi_2O_6$, 3% for $CaAl_2Si_2O_8$ [23,24]. MacPherson et al. [12] used similar arguments to conclude that the amount of porosity in blue spinel-hibonite spherules in Murchison is also consistent with crystallization from a melt. The one spinel-rich object (Fig. 3A) with a Ca, Si-rich core surrounded by spinel and a rim sequence could have originated by spinel grains

adhering to the surface of a melt globule.

The differences in the FeO content of the spinels in spinel-rich objects in Kaba, Allende, and Mokoia could represent differences in the redox state of regions in the nebula where these objects formed or could represent different amounts of alteration after formation (either in the nebula or in parent bodies), (cf. Kornacki and Wood [8]; Bischoff and Keil [25]). McSween [6] concluded that both Kaba and Mokoia were less metamorphosed than Allende; he also found that FeO contents of "fine-grained" Kaba and Mokoia CAI's were lower than the FeO contents of "fine-grained" Allende CAI's [7]. Assuming that the hedenbergite in the Kaba CAI is due to nebular alteration, the presence of an abundant FeO-bearing phase surrounding FeO-poor, spinel-rich objects also indicates little metamorphic alteration of the CAI (or else the spinels would have higher FeO contents). In this view the higher FeO contents of the Allende spinel-rich objects is simply the results of planetary metamorphism.

Alternatively, the spinel-bearing objects in Kaba and Mokoia formed in a less oxidizing region of the nebula than did the spinel nodules in Allende. Kornacki and Wood [8] presented persuasive evidence that the high FeO content of the spinels is not due to alteration of metallic Fe or Fe-bearing sulfides. Measurement of the abundances of the Pt-metals, W, and Mo in Allende, Mokoia, and Kaba CAI's could resolve this question because Fegley and Palme [26] suggested that Mo and W depletions (relative to Pt-group metals of similar volatilities) in CAI's are indicators of the redox state of the solar nebula. However, these data are unavailable for the CAI's studied.

5.4. Condensation as an alternative model

Although the textural and mineralogical features of spinel-rich objects in Kaba are consistent with Cohen's model, they do not unambiguously rule out of possibility that at least some of the spinel nodules have a condensation origin. For example, Kornacki and Fegley [17] noted that the reaction of melilite with nebular gas at $T \approx 1450$ K ($P = 10^{-3}$ bars) should produce spinel and diopside intergrown with a reaction texture and sometimes rimming relict cores of melilite. Superficially similar textures are found in several of the spinel-rich objects in Kaba, especially in one which has a section of melilite around a portion of the circumference of the core (Fig. 3C).

However, there are some problems with a condensation origin. Except for the relict melilite partially rimming a portion of the core of one object (Fig. 3C), none is found associated with the intergrown spinel and pyroxene. If the melilite in this nodule were a relict of a vapor–solid reaction to produce spinel + pyroxene, we would expect it to be in the center of the core and not partially rimming it because the reaction would proceed from the outside of the putative melilite precursor to the inside. Second, as noted by Kornacki and Fegley [17], since Ca and Al should be totally condensed at 1450 K, the resulting (intergrown) spinel + pyroxene assemblage should have the cosmic CaO/Al_2O_3 ratio. Initial segregation of a Ca-rich condensate is not an effective method for fractionating Ca and Al because the major Ca-bearing condensate (and CAI mineral) is melilite, which is also the major Al-bearing condensate [17]. However our microprobe data show that the cores of the concentric objects have CaO/Al_2O_3 ratios *lower* than the solar value (see Table 1). Even if all the porosity (≈ 5–10%) in the cores of the spinel-rich objects is due to plucking of pyroxene during sample preparation, the CaO/Al_2O_3 ratios are still substantially lower than the solar value.

Alternatively, the spinel nodules could have lost Ca by secondary alteration, possibly by reaction of melilite with CO_2(g) to give diopside and calcite (which was then lost) [27]. However relict melilite is found in only one spinel body. Also, the calculated CO_2 partial pressure in the solar nebula [28] is several orders of magnitude too low to produce diopside from melilite. Alteration on chondrite parent bodies is a possibility, but the similarity of the spinel-rich objects found in C2, C3, and ordinary chondrites suggests that they were formed in the solar nebula. Finally, we note that extensive theoretical and experimental arguments have been made against the condensation of crystalline minerals in a hot solar nebula [14,17,29] and references therein). Thus we conclude that the spinel-rich objects in Kaba probably did not originate by vapor–solid condensation.

5.5. *Possible constraints on nebular and planetary processes*

The observed properties of the Kaba CAI in principle define several constraints on specific nebular and planetary processes including the proposed melting of the spinel-rich objects, their residence time in hot regions of the solar nebula, the rimming of the spinel-rich objects, the accretion of the entire CAI, and its subsequent thermal history. However, the utility of these constraints cannot be completely exploited at present because of the lack of all the necessary quantitative data (such as the relevant diffusion coefficients for Ti-Al coupled diffusion in pyroxene). Therefore we will only briefly mention some implications of these constraints.

The Ti-Al pyroxenes in the cores of the spinel-rich objects are heterogeneous on length scales of ≈ 5–10 μm, while the spinels in the cores are effectively homogeneous on similar length scales. These observations in principle could be used to constrain the thermal histories of the spinel-rich objects. The data of Freer and O'Reilly [30] on Fe^{2+} diffusion in polycrystalline $FeAl_2O_4$-$MgAl_2O_4$ spinels indicates that homogenization is very rapid. For example, at 1450 K (where spinel + diopside form by reaction of melilite with nebular gas at 10^{-3} bars), 10 μm spherical spinel grains would be homogenized in only 1 minute (estimated using $x^2 \simeq Dt$ where x is the radius, D is the diffusion coefficient for 5 wt.% Fe [30] and t is time). However, by analogy with CaAl-NaSi coupled diffusion in plagioclase [31], 10 μm spherical Ti-Al pyroxene grains would require 2800 years to be homogenized. It may be the case that coupled Ti-Al diffusion in CAI pyroxenes is too slow to be a useful thermal history indicator, except at high temperatures. Taking Cameron's [32] estimate of 10^{13} seconds for the nebular cooling time, we estimate that 10 μm spherical Ti-Al pyroxene grains will not homogenize over this time unless $D \geqslant 2.5 \times 10^{-20}$ cm^2 s^{-1}. The CaAl-NaSi interdiffusion coefficient in plagioclase [31] and the Ca-Mg interdiffusion coefficient in sub-calcic diopside [33] are of this magnitude at 1300 K, and the Ti-Al interdiffusion coefficient in CAI pyroxenes may have a similar value. Thus, the pyroxene and spinel concentration variations are consistent with the expected diffusion coefficients but insufficient data are available to provide firm constraints on the thermal history of the spinel-rich objects.

However, the rims on the spinel-bearing objects may pose more stringent constraints on the accretion of the CAI and its subsequent thermal history. The sharp compositional boundary between the diopside and hedenbergite rims on the spinel nodules and between the diopside rim and hedenbergite veins and patches precludes long residence times at high temperatures for the Kaba CAI. Nord et al. [34] first used rim mineralogies to constrain the thermal histories of CAI's; they concluded that the coexistence of wollastonite and hedenbergite in a Type A rim indicated alteration (to form the rim) at < 1048 K. Taking $D(Fe^{2+}) \leqslant 2 \times 10^{-11}$ cm^2 s^{-1} at 1423 K from Brady and McCallister [33] and assuming activation energies ranging from 30 to 90 kcal/mole for Fe^{2+} diffusion in diopside, $D \leqslant 2.5 \times 10^{-14}$ to 3.9×10^{-20} cm^2 s^{-1}, respectively, at 873 K. This temperature probably is representative of peak metamorphic temperatures in CV3 chondrites [6]. The corresponding times for homogenization of a 5 μm thick rim layer are 116 days to 2×10^5 years, respectively. Thus the preservation of the distinct diopside-hedenbergite rims indicates either relatively cool accretion and a subsequently cool thermal history with only a very brief time at the peak metamorphic temperature or extremely slow Fe^{2+}-Mg^{2+} chemical interdiffusion. Although the latter possibility cannot be unambiguously ruled out on the basis of available data, other qualitative indicators also point toward a cool thermal history for the Kaba CAI. For example, the presence of distinct grains with sizes $\leqslant 10$ μm in the CAI matrix material indicates that extensive sintering did not occur. Since sintering of small grain size materials is a rapid process (minutes) at $T \geqslant 1000$ K [35,36], the existence of separate grains is incompatible with even relatively short times at high temperatures. We note that analogous arguments have been made by Armstrong et al. [37] who used mineralogical heterogeneities in Fremdlinge to constrain the thermal histories of their host CAI's.

6. Summary

Our work on this "fine-grained" CAI in Kaba is the first detailed description of a CAI in this meteorite. Our study of the rimmed, rounded

spinel-cored objects shows that they have important morphological and mineralogical similarities to rimmed, rounded spinel-cored bodies in Allende, Mokoia, other carbonaceous chondrites, and ordinary chondrites. Our conclusions thus confirm the assertion of Kornacki and Fegley [17] that important similarities exist between spinel-rich objects in different meteorites. However, we also observed subtle differences between the spinel-rich bodies in Kaba and Allende. The former are composed of FeO-poor spinel, do not contain abundant feldspathoids, and have a hydrous silicate rim, while the latter contain pleonaste spinel, abundant feldspathoids, and no hydrous silicates. In these respects the Kaba and Mokoia spinel-cored objects are similar.

Second, our interpretation of the petrographic and mineralogical data tends to support an origin of the spinel-rich objects in Kaba as fractionated distillation residues of primitive dust. Because similar objects in Allende [8], Mokoia [14] and Murchison [12] have also been interpreted as fractionated igneous residues it is probable that a common process was a widespread occurrence in the solar nebula. Bischoff and Keil [25] argued in an analogous fashion that all chondrules (Al-rich and Mg-Fe-rich) formed by related mechanisms. If similar mechanisms are responsible for the origin of spinel-rich objects (whether they occur as individual "chondrules" or as constituents of CAI's), then constraints on these important chemical and physical processes are very desirable. However, some potential constraints such as Ti-Al heterogeneity in fassaitic pyroxenes are not useful at present because the relevant diffusion coefficients are unknown. However, qualitative constraints based on the sharp diopside-hedenbergite boundary in the rims on spinel-rich objects and the small grain size of the CAI matrix suggest a relatively cool thermal history for this CAI.

Acknowledgements

We thank J.A. Peck and A.S. Kornacki for bringing this CAI to our attention and J.A. Wood for generously loaning us the section for study. We also thank A.S. Kornacki and G.J. MacPherson for helpful comments and E. Seling for some SEM micrographs. B.F. acknowledges support from the NASA Planetary Materials and Geochemistry program (R. Prinn, PI), NSF grant ATM-84-01232 to MIT, and to R.L. Pober and H.K. Bowen, CPRL, MIT. J.E.P. was partially supported by NSF grant EAR-792-005 to C.W. Burnham, Harvard. We thank J. Sloman for preparation of the manuscript.

References

1 J. von Török, Ueber den Kaba-Debreczin-Meteorit, Ann. Phys. Chem. Poggendorff, Ser. IV 15, 329–334, 1858.
2 K.I. Sztrokay, V. Tolnay and M. Foldvari-Vogl, Mineralogical and chemical properties of the carbonaceous meteorite from Kaba, Hungary, Acta Geol. (Hungary) 7, 57–103, 1961.
3 U.B. Marvin, J.A. Wood and J.S. Dickey, Jr., Ca-Al rich phases in the Allende meteorite, Earth Planet. Sci. Lett. 7, 346–350, 1970.
4 M. Christophe Michel-Levy, Un chondre exceptionnel dans la météorite de Vigarano, Bull. Soc. Fr. Mineral. Cristallogr. 91, 212–214, 1968.
5 M.J. Frost and R.F. Symes, A zoned perovskite-bearing chondrule from the Lance meteorite, Mineral. Mag. 37, 724–726, 1970.
6 H.Y. McSween, Jr., Petrographic variations among carbonaceous chondrites of the Vigarano type, Geochim. Cosmochim. Acta 41, 1777–1790, 1977.
7 H.Y. McSween, Jr., Chemical analyses of chondrules and inclusions in chondritic meteorites, unpublished results, 1977.
8 A.S. Kornacki and J.A. Wood, Mineral chemistry and origin of spinel-rich inclusions in the Allende CV3 chondrite, Geochim. Cosmochim. Acta 49, 1219–1237, 1985.
9 G.J. MacPherson and L. Grossman, "Fluffy" Type A Ca, Al-rich inclusions in the Allende meteorite, Geochim. Cosmochim. Acta 48, 29–46, 1984.
10 B. Fegley, Jr., J.E. Post and J.A. Peck, Mineral chemistry of a large spinel-rich inclusion in the Kaba CV3 chondrite (abstract), Lunar Planet. Sci. XV, 264–265, 1984.
11 C.S. Smith and L. Guttman, Measurement of internal boundaries in three-dimensional structures by random sectioning, Trans. AIME 197, 81–87, 1953.
12 G.J. MacPherson, M. Bar-Matthews, T. Tanaka, E. Olsen and L. Grossman, Refractory inclusions in the Murchison meteorite, Geochim. Cosmochim. Acta 47, 823–839, 1983.
13 D.A. Wark and J.F. Lovering, Marker events in the early evolution of the solar systems: Evidence from rims on Ca-Al-rich inclusions in carbonaceous chondrites, Proc. 8th Lunar Planet. Sci. Conf., pp. 95–112, 1977.
14 R.E. Cohen, A.S. Kornacki and J.A. Wood, Mineralogy and petrology of chondrules and inclusions in the Mokoia CV3 chondrite, Geochim. Cosmochim. Acta 47, 1739–1757, 1983.
15 D.A. Wark and J.F. Lovering, The nature and origin of type B1 and B2 Ca-Al-rich inclusions in the Allende meteorite, Geochim. Cosmochim. Acta 46, 2581–2594.
16 A.S. Kornacki and J.A. Wood, Petrography and classification of Ca, Al-rich and olivine-rich inclusions in the Allende CV3 chondrite, Proc. 14th Lunar Planet. Sci. Conf., J. Geophys. Res. 89, B573–B587, 1984.

17 A.S. Kornacki and B. Fegley, Jr., Origin of spinel-rich chondrules and inclusions in carbonaceous and ordinary chondrites, Proc. 14th Lunar Planet. Sci. Conf., J. Geophys. Res. 89, B588–B596, 1984.
18 D.A. Wark, Birth of the presolar nebula: the sequence of condensation revealed in the Allende meteorite, Astrophys. Space Sci. 65, 275–295, 1979.
19 R. Cohen, Concentric objects in C2 and C3 carbonaceous chondrites (abstract), Meteorit. Soc. Meet., Bordeaux, 1985.
20 A.A. Ulyanov, On the origin of fine-grained Ca, Al-rich inclusions in the Efremovka carbonaceous chondrite (abstract), Lunar Planet. Sci. XV, 872–873, 1984.
21 R.E. Cohen, Refractory inclusions in the Mokoia C3(V) carbonaceous chondrite (abstract), Meteoritics 16, 304, 1981.
22 E. Stolper, Crystallization sequences of Ca, Al-rich inclusions from Allende: an experimental study, Geochim. Cosmochim. Acta 46, 2159–2180, 1982.
23 T. Licko and V. Danck, Densities of melts in the system $CaSiO_3$-$CaMgSi_2O_6$-$Ca_2MgSi_2O_7$, Phys. Chem. Glasses 23, 67–71, 1982.
24 H.S. Yoder, Jr., Generation of Basaltic Magma, 265 pp., National Academy of Sciences, 1976.
25 A. Bischoff and K. Keil, Al-rich objects in ordinary chondrites: Related origin of carbonaceous and ordinary chondrites and their constituents, Geochim. Cosmochim. Acta 48, 693–709, 1984.
26 B. Fegley, Jr. and H. Palme, Evidence for oxidizing conditions in the solar nebula from Mo and W depletions in refractory inclusions in carbonaceous chondrites, Earth Planet. Sci. Lett. 72, 311–326, 1985.
27 J.T. Armstrong, G.P. Meeker, J.C. Huneke, and G.J. Wasserburg, The Blue Angel I. The mineralogy and petrogenesis of a hibonite inclusion from the Murchison meteorite, Geochim. Cosmochim. Acta 46, 575–595, 1982.
28 J.S. Lewis, S.S. Barshay and B. Noyes, Primordial retention of carbon by the terrestrial planets, Icarus 37, 190–206, 1979.
29 A.G.W. Cameron and M.B. Fegley, Nucleation and condensation in the primitive solar nebula, Icarus 52, 1–13, 1982.
30 R. Freer and W. O'Reilly, The diffusion of Fe^{2+} ions in spinels with relevance to the process of maghemitization, Mineral. Mag. 43, 889–899, 1980.
31 T.L. Grove, M.B. Baker and R.J. Kinzler, Coupled CaAl-NaSi diffusion in plagioclase feldspar: experiments and applications to cooling rate speedometry, Geochim. Cosmochim. Acta 48, 2113–2121, 1984.
32 A.G.W. Cameron, Physics of the primative solar accretion disk, Moon Planets 18, 5–40, 1978.
33 J.B. Brady and R.H. McCallister, Diffusion data for clinopyroxenes from homogenization and self-diffusion experiments, Am. Mineral. 68, 95–105, 1983.
34 G.L. Nord, Jr., J.S. Heubner and J.J. McGee, Thermal history of a Type A Allende inclusion (abstract), EOS 63, 462, 1982.
35 E.A. Barringer and H.K. Bowen, Formation, packing, and sintering of monodisperse TiO_2 powders, J. Am. Ceram. Soc. 65, C199–C201, 1982.
36 C. Herring, Effects of change of scale on sintering phenomena, J. Appl. Phys. 21, 301–303, 1950.
37 J.T. Armstrong, A. El Goresy and G.J. Wasserburg, Willy: A Prize Noble Ur-Fremdling—Its history and implications for the formation of Fremdlinge and CAI, Geochim. Cosmochim. Acta 49, 1001–1002, 1985.